Journal of Molecular Spectroscopy 251 (2008) 185–193

Contents lists available at ScienceDirect

Journal of Molecular Spectroscopy

journal homepage: www.elsevier.com/locate/jms

The rotational spectrum of the NF_2 free radical: Determination of molecular structure

Holger S.P. Müller [a], Kai Löblein [b], Hans Hübner [b], Wolfgang Hüttner [b], John M. Brown [c,*]

[a] I. Physikalisches Institut, Universität zu Köln, 50968 Köln, Germany
[b] Universität Ulm, Institut für Quanteninformationsverarbeitung, 89069 Ulm, Germany
[c] The Physical and Theoretical Chemistry Laboratory, Department of Chemistry, The University of Oxford, South Parks Road, Oxford OX1 3QZ, UK

ARTICLE INFO

Article history:
Received 21 December 2007
In revised form 18 February 2008
Available online 29 February 2008

This work is dedicated to Edward A. Cohen and Herbert M. Pickett in recognition of their many contributions to the theory and application of molecular spectroscopy.

Keywords:
Rotational spectroscopy
Free radical
Ab initio calculations
Molecular structure
^{14}N hyperfine parameters
^{19}F hyperfine parameters
Nitrogen difluoride
Ortho–para mixing

ABSTRACT

Many rotational transitions of nitrogen difluoride, NF_2, have been recorded in the millimetre-wave region. By fitting the present and previous data together, it has been possible to determine several higher order centrifugal distortion terms and so refine the rotational and spin-rotational parameters. In addition, it has been possible to determine the off-diagonal electron spin–nuclear spin coupling parameter T_{ab} for the two equivalent ^{19}F nuclei. This term causes *ortho–para* mixing and, to our knowledge, this is the first time that such a term has been determined directly by spectroscopic means for spin 1/2 nuclei. Density- and wave-functional calculations employing moderately large to large basis sets have been carried out to test the reliability of such calculations and to corroborate the experimental hyperfine structural findings. In addition, vibration–rotation interaction terms were calculated theoretically in order to derive a mixed experimental/*ab initio* equilibrium structure for NF_2 in the X^2B_1 state, namely:
$r = 134.691(68)$ pm and $\angle = 103.132(20)^\circ$.

1. Introduction

The NF_2, nitrogen difluoride or difluoroamidogen, radical in its $^2B_1$ ground state is a member of a small class of free radicals that are chemically stable. It was first identified by Johnson and Colbourn in 1961 [1] with the discovery that it exists in equilibrium with tetrafluorohydrazine, N_2F_4 (which they had just synthesised); it can be made readily in high concentration simply by heating a sample of N_2F_4. The first spectroscopic studies of NF_2 were made in the infrared and microwave regions very soon after its discovery.

In the infrared region, Harmony et al. [2] measured the symmetric (ν_1) and anti-symmetric (ν_3) stretching wavenumbers to be 1075 and 930 cm^{-1}, respectively; the bending vibration (ν_2) wavenumber was measured as 573 cm^{-1} in a nitrogen matrix at 20 K [3]. The ν_1 and ν_3 bands were later recorded at much higher resolution by diode laser spectroscopy by Davies et al. [4] and by Davies and Hamilton [5], respectively. Analysis of these results yielded molecular parameters for the molecule in the two excited vibrational levels, including the Coriolis coupling coefficient, $\zeta_{13}^{(c)}$, between them. A few transitions in the ν_1 band were also recorded by CO_2 laser magnetic resonance by Hakuta and Uehara [6], who exploited avoided level-crossings between adjacent rotational levels to endow the magnetically tuneable transitions with electric-dipole intensity.

The first observations of the rotational spectrum of the NF_2 radical were made by Hrubesh et al. [7] in the frequency region around 26 GHz. This was followed by a much more extensive study by Brown et al. [8] who recorded the spectrum between 13 and 62.5 GHz. The frequencies that they measured were analysed and used to determine a set of molecular parameters. This consisted of values for the rotational constants, four centrifugal distortion parameters and eleven other parameters that describe the electron spin-rotation and ^{14}N and ^{19}F hyperfine effects. They also determined the electric dipole moment ($\mu_b = 0.136 \pm 0.010$ D) from Stark effect measurements. The rotational spectrum of NF_2 has also been studied in the presence of large and variable magnetic fields by Frank and Hüttner [9]. The work had the specific objective of identifying transitions that are insensitive to linear paramagnetic Zeeman effects (so-called magic doublets [10]). The main result of this study was an accurate determination of the electron-spin

* Corresponding author. Fax: +44 1865 275410.
E-mail addresses: jmb@physchem.ox.ac.uk, john.m.brown@chem.ox.ac.uk (J.M. Brown).

0022-2852/$ - see front matter © 2008 Elsevier Inc. All rights reserved.
doi:10.1016/j.jms.2008.02.014

and rotational g-factors of NF_2 in its ground state. The rotational and hyperfine parameters were re-determined by including the magic doublet zero-field transition frequencies in the fit. Uehara and Horiai have also measured a rotational interval of NF_2 in its ground state (3_{03}–2_{12}) in a microwave-infrared double resonance experiment in the presence of a magnetic field [11], using some of the avoided level crossings in the ν_3 band. The main result was an accurate measurement of the electronic g-tensor anisotropies, consistent with the work of Frank and Hüttner [9].

One of the objectives of the present work was to investigate whether mixing of *ortho* and *para* levels could be identified in NF_2. Curl et al. [12] were the first to point out that, unlike H_2, the *ortho* and *para* levels of non-linear molecules with equivalent identical nuclei are not independent of each other. They showed that *ortho* and *para* rotational levels are connected by the nuclear spin–rotation interaction and in some cases by spin–spin coupling. Though these interactions are small in magnitude (on the order of kHz), they become important if there is an appropriate accidental degeneracy. In this situation, they provide routes for one spin-modification to funnel through to the other. Consequently, it is virtually impossible to achieve and retain a non-equilibrium isotopic mixture of such molecules at any reasonable temperature. In a microwave study of CH_2Br_2, Chadwick and Millen [13] showed that similar *ortho*/*para* mixing can occur through the nuclear electric quadrupole interaction. The coupling in this case can be much larger, about 400 MHz in the case of CH_2Br_2. Since this first observation, many other instances of electric quadrupole coupling of *ortho* and *para* levels have been identified, see for example Br_2O [14,15].

All of the above coupling phenomena refer to closed-shell molecules. For an open-shell molecule like NF_2, other hyperfine interactions that involve the electron spin become available to mix *ortho* and *para* levels. Let us consider the electron spin–nuclear spin dipole–dipole coupling term in the molecular Hamiltonian for an open-shell molecule with two equivalent nuclei. This interaction can be written in Cartesian tensor form as

$$\mathscr{H}_{\mathrm{dip}} = \boldsymbol{I}_1 \cdot \boldsymbol{T}_1 \cdot \boldsymbol{S} + \boldsymbol{I}_2 \cdot \boldsymbol{T}_2 \cdot \boldsymbol{S} \tag{1}$$

$$= \frac{1}{2}\boldsymbol{I}_{\mathrm{T}} \cdot (\boldsymbol{T}_1 + \boldsymbol{T}_2) \cdot \boldsymbol{S} + \frac{1}{2}(\boldsymbol{I}_1 - \boldsymbol{I}_2) \cdot (\boldsymbol{T}_1 - \boldsymbol{T}_2) \cdot \boldsymbol{S}, \tag{2}$$

where $\boldsymbol{S}$ is the electron spin, $\boldsymbol{I}_1$ and $\boldsymbol{I}_2$ are the (identical) nuclear spins of the equivalent nuclei labelled 1 and 2, $\boldsymbol{T}_1$ and $\boldsymbol{T}_2$ are the corresponding dipolar coupling 2nd rank tensors, and $\boldsymbol{I}_{\mathrm{T}}$ is the total coupled spin

$$\boldsymbol{I}_{\mathrm{T}} = \boldsymbol{I}_1 + \boldsymbol{I}_2. \tag{3}$$

It can be seen that the non-zero matrix elements of the first term on the right-hand side of Eq. (2) are diagonal in I_{T} and therefore preserve the *ortho*/*para* character. The non-zero matrix elements of the second term are off-diagonal in I_{T} by 1 (in fact by any odd integer) and can therefore lead to a mixing of the *ortho* and *para* levels. Such mixing does require some of the elements of the difference tensor $(\boldsymbol{T}_1 - \boldsymbol{T}_2)$ to be non-zero. The diagonal elements are zero because the two nuclei are equivalent but the off-diagonal are not necessarily zero. In the case of NF_2, only the component $(\boldsymbol{T}_1 - \boldsymbol{T}_2)_{ab} \equiv T_{ab}$ is non-zero by symmetry.

In the present paper, we present additional measurements of the rotational spectrum of NF_2 in its ground state in the millimetre-wave region. These measurements have been combined in a weighted fit that takes all the available field-free data on the rotational spectrum into account to determine an essentially complete set of molecular parameters. In particular we have determined the value of the dipolar hyperfine parameter T_{ab} for the ^{19}F nuclei; this is the first time that such a term in the effective Hamiltonian has been identified for a symmetrical molecule.

2. Experimental details

The NF_2 radical was produced in the absorption cell by pyrolytic decomposition of the stable molecule N_2F_4 at 92 °C. This temperature was found to be the best compromise between a high concentration and unwanted population of excited vibrational levels of NF_2 [16]. The preparation of N_2F_4 has been described previously [9].

The microwave absorption cell was located in a 1.82 m long H frame electromagnet providing a transverse magnetic field. The cell had been used previously for Zeeman-effect measurements; it contains a Stark septum 1.20 m in length, chosen to avoid the effect of modulation in the outer, inhomogeneous-field regions. Many lines of the paramagnetic species NF_2 are field-sensitive, showing broadening and even splitting in the earth's magnetic field. Accordingly, the magnet was used for shielding purposes in the present zero-field investigations; the local field was cancelled out by application of the appropriate current. The cell is made of copper and was passivated by filling it with hot N_2F_4/NF_2 gas mixtures at pressures up to 5 kPa. Under these conditions, a surface layer of copper difluoride is formed that prevents decomposition of NF_2 without diminishing the transmission of microwaves noticeably. The cell was heated by flowing a commercial mixture of di-benzyl toluene isomers (Ultra-Therm 330 SCB) through tubes fastened along both sides of the cell. The whole assembly was wrapped loosely with several layers of insulation material (NRC-2-super isolation foil).

Rotational levels of NF_2 up to $N = 32$ have been investigated. Transitions involving these high-N levels are usually barely detectable with the Stark modulation technique even with a maximum amplitude of the sinusoidal field of almost 7×10^5 V/m. Most of the lines were therefore recorded using 10 kHz, 2f-detected source modulation. The effective absorption path length was 1.90 m. A liquid-He cooled InSb hot-carrier bolometer, type QFI/2, was used for detection. The weakest securely assigned line measured this way shows a (calculated) absorption coefficient of $\alpha \approx 1 \times 10^{-8}\,\mathrm{cm}^{-1}$; it required a sampling time of more than one hour. Gas pressures ranged between 3 and 4 Pa and the typical line width (FWHM) was of order of 300 kHz; the line-shape is the second derivative of a Doppler profile (see Fig. 1 for an example of a comparatively strong line).

The frequency interval between 96 and 169 GHz was covered with klystrons as primary sources combined with multiplication techniques. The klystrons were stabilized by two phase-lock loops

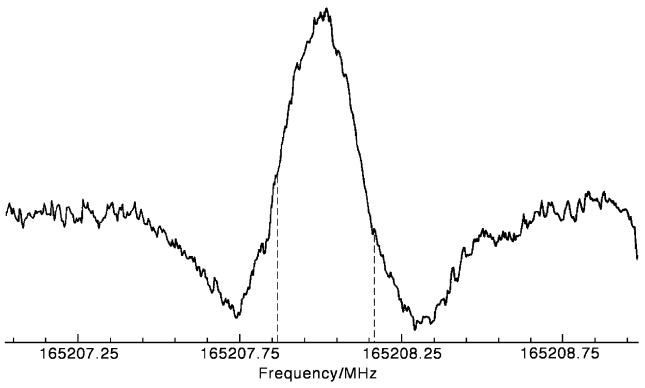

Fig. 1. A recording of a single hyperfine component in the millimetre wave spectrum of NF_2. The transition has been assigned as $N_{K_aK_c} = 16_{2,14}$–$16_{1,15}$, $J = 15^1_2$–15^1_2, $F_1 = 16^1_2$–16^1_2, $F = 15^1_2$–15^1_2; the line centre is measured to be 165208.019 MHz. The pressure in the sample cell was 3.5×10^{-2} mbar and the spectrum is the average of two scans each with an output time constant of 1 s. The modulation frequency was 10 kHz and the modulation amplitude 360 kHz. The separation between the two dashed lines is 300 kHz.

(PLL) in series. The output of a backward wave oscillator (Marconi sweeper 6600 A) was locked to a frequency generator Marconi 2019 A (80 kHz...1024 MHz) and used as the local oscillator for the klystron. Two frequency phase discriminators of the type FDS 30 were employed, with somewhat different working frequencies (30 and 29.85 MHz for PPL1 and PPL2, respectively). The 29.85 MHz discriminator frequency was modulated at a frequency of 10 kHz when the 2*f*-detected frequency modulation mode was used, using a variable amplitude.

The frequency of the quartz crystal of the primary standard was checked against the carrier of the radio station Mainflingen (77.5 kHz, 10^{-9}); the consequent uncertainty of the locked klystron frequencies is less than 1 kHz. This is negligibly small compared with a typical line width. The frequency-modulated recording of a single hyperfine component of the *ortho* transition $16_{2,14}$–$16_{1,15}$, $J = 15^1_2$—15^1_2, $F_1 = 16^1_2$—16^1_2, $F = 15^1_2$—15^1_2, near 165208 MHz, is shown in Fig. 1. The calculated absorption coefficient is $\alpha = 1.1 \times 10^{-6}$ cm^{-1} and the sampling time was 4 min.

3. Theoretical calculations

Both density- and wave-functional *ab initio* calculations have been carried out at the Regionales Rechenzentrum Köln in the Zentrum für Angewandte Informatik (Centre for Applied Informatics) of the Universität zu Köln. The familiar hybrid density functional B3LYP as well as MP2 second order perturbation theory calculations have been performed to obtain spin–spin coupling parameters for ^{19}F as well as for ^{14}N and to calculate vibration–rotation interaction terms α_i^g (i = 1, 2, 3 for the three fundamental vibrations of NF_2; g = *A*, *B*, *C*). The latter are used to derive mixed experimental/*ab initio* equilibrium rotational constants from the experimentally determined zero-point values which in turn yield equilibrium structural parameters. All calculations have been carried out at the respective theoretical equilibrium structure. Structure calculations have also been performed at the coupled cluster level CCSD(T) which considers single and double excitations with connected triple excitations taken into account perturbatively. The correlation-consistent basis sets cc-pVXZ of triple, quadruple and, for B3LYP calculations only, quintuple zeta quality (X = T, Q, 5) [17] were used in the calculations. One set of diffuse basis functions (aug-cc-pVXZ) [18] has been used frequently, two sets (daug-cc-pVXZ) [19] have been employed only rarely. The effects of core-correlating basis functions ({aug-}cc-pwCVXZ) [20] were also tested frequently. In the course of MP2 or CCSD(T) calculations, the core electrons were generally not correlated. In some instances all electrons were correlated; these calculations are denoted with an (ae) after the basis set. All theoretical calculations were carried out with the Gaussian03 [21] programme.

4. Observed spectrum and analysis

4.1. Hamiltonian and basis set

The nitrogen difluoride radical is an asymmetric top with $\kappa = -0.9425$, fairly close to the prolate symmetric limit of −1. It has a $^2B_1$ electronic ground state and the small dipole moment of about 0.14 D [8] lies along the *b*-axis. The effective Hamiltonian required to describe the energy levels of NF_2 consists of three parts:

$$\mathscr{H} = \mathscr{H}_{\rm rot} + \mathscr{H}_{\rm fs} + \mathscr{H}_{\rm hfs}, \tag{4}$$

where $\mathscr{H}_{\rm rot}$ is a Watson *S*-reduction of the rotational Hamiltonian in the I^r representation [22] that contains an almost complete set of sextic centrifugal distortion terms; $\mathscr{H}_{\rm fs}$ is the fine structure Hamiltonian describing the electron spin-rotation with some quartic centrifugal distortion terms; and $\mathscr{H}_{\rm hfs}$ is the fairly complex hyperfine structure Hamiltonian that describes effects caused by the ^{14}N and ^{19}F nuclei. Since most of the parameters employed in the current fit are very familiar, they do not need stating explicitly.

Watson's *S*-reduction of the rotational Hamiltonian [22] is a natural choice for a molecule so close to the symmetric prolate limit as NF_2 even though the *A*-reduction has been used in the past. The *S*-reduction also resulted in a somewhat better fit for the present data set and the T_{ab} term was less correlated, leading to much smaller variations of its value in the fits.

We have chosen to couple the rotational, electron spin, and nuclear spin angular momenta as follows:

$$\boldsymbol{N} + \boldsymbol{S} = \boldsymbol{J}, \tag{5}$$

$$\boldsymbol{J} + \boldsymbol{I_N} = \boldsymbol{F}_1, \tag{6}$$

$$\boldsymbol{I_{F1}} + \boldsymbol{I_{F2}} = \boldsymbol{I_F}, \tag{7}$$

$$\boldsymbol{F}_1 + \boldsymbol{I_F} = \boldsymbol{F}. \tag{8}$$

The order in which the two nuclear spin angular momenta have been coupled was dictated by the programmes used to predict and fit the NF_2 rotational spectrum [23]. The order is different from the previous analyses which recognised the generally much larger hyperfine structure effects in *ortho*-NF_2 caused by the ^{19}F nuclei compared with the effects of ^{14}N.

The angular momentum from the unpaired electron causes each rotational level to be split into two. The nuclear spin of the ^{14}N nucleus, $I_N = 1$, splits each sublevel further into three. Each sublevel having $K_a + K_c$ = even is further split into three because of the two equivalent ^{19}F nuclei ($I_F = 1$; *ortho*-NF_2) while those having $K_a + K_c$ = odd show no further splittings ($I_F = 0$; *para*-NF_2). The fine and hyperfine structure effects thus give rise to a large number of components for each rotational transition. For example, there are 48 hyperfine components of the 2_{11}–2_{02} transition in the final line list. However, for larger values of N the strongest transitions are described by $\Delta F = \Delta F_1 = \Delta J = \Delta N$, resulting in 3 and 9 strong hyperfine components for each of the two strong fine structure components for *para*- and *ortho*-NF_2, respectively.

4.2. Assignments and least-squares fits

The assignment of the new millimetre-wave observations was straightforward, being reliably guided by predictions based on the previously determined parameters [8,9]. The three parts of the data set were assessed separately before being combined in the final weighted least-squares fit. The versatile spfit program written by Pickett [23] was used for this purpose; the weights were taken as the inverse square of the experimental uncertainty. In the preliminary fits of the previous measurements [8,9], blocks of frequencies showed residuals that were larger than the authors' estimated experimental uncertainty (95% confidence limits). We have adjusted the uncertainties in these cases as described below. Because the data set reported by Brown et al. [8] is rather extensive and involves many low-*N* transitions, these lines were fitted first. The initial spectroscopic parameters were taken from Ref. [9] with as many parameters as possible kept fixed in the early stages of the analysis. Using uncertainties of 30 kHz for lines given with 10 kHz digits and 100 kHz for those given only with 100 kHz digits in Ref. [8], almost all the lines could be fitted with an rms error relative to the experimental uncertainties of slightly less than 1.0. The smaller of the two uncertainties is somewhat larger than the value of 10 kHz estimated by Brown et al. [8]. Even with this adjustment of the uncertainties, there remain a few lines with residuals three times larger than their uncertainties at this stage in the fit; these measurements were judged to be unreliable by this criterion and so were excluded from the final fit. The transition frequencies reported by Brown et al. [8] with uncertainties of 1 or 10 MHz were

also excluded from the fit as these contributed insignificantly to the spectroscopic parameters. When the magic doublet transition frequencies reported by Frank and Hüttner [9] were included in the fit with the authors' estimated uncertainties, the relative standard deviation of these transitions was almost 4.0. It is possible that the effects of incomplete Stark effect modulation caused systematic line shifts in these measurements which dominated the random error. In the final fit of the data from Ref. [9], the error estimates of these lines were therefore increased by a factor of 4. Finally, the newly measured transition frequencies, which were almost all recorded using the frequency modulation technique, were included in the fit with their estimated uncertainties ranging from 10 to 50 kHz. The assignments of the weakest lines recorded, more than one hundred times weaker than the strongest ones, had to be scrutinised very carefully since not only transitions of NF_2 in the lowest excited $v_2 = 1$ state but also those in $v_1 = 1$, $v_3 = 1$, and $v_2 = 2$ levels can have intensities of comparable or greater intensity. Accidental overlap with vibrationally excited lines may affect the measured line positions appreciably. A small number of the newly recorded transitions were omitted from the fit because the large residuals of these lines with respect to other lines from the respective transition suggested they were indeed overlapped. The very weak $23_{2,21}$–$24_{1,24}$ transition proved to be a particularly difficult one to assess. In this case, a pattern of six lines consisting of two hyperfine triplets is expected. Although the hyperfine splittings are reliably predictable, the fine structure separation for this high-N transition is less so (to the extent of a few tens of kHz). Only two of the six lines could be identified in the observed spectrum. These two lines were retained in the fit because they had the correct hyperfine separation and were of the expected intensity; the third member of this group was lost in the noise. The other hyperfine triplet was predicted to fall in a region of the spectrum (some 1350 MHz higher) where the signal-to-noise ratio was too low for its detection. Although the inclusion of the two retained transition frequencies should be viewed with some caution, it had the merit that it improved the determination of the rotational centrifugal distortion parameters.

The final line list consists of 437 different spectral features corresponding to 479 hyperfine components some of which are overlapped. As it was difficult to determine a unique set of spectroscopic parameters, care was taken to include only those parameters that were both well determined (having an uncertainty less than 20% of the value) and whose use in the fit contributed to the reduction of the rms error of the fit. On this basis, the remaining sextic distortion term H_N was omitted from the final fit. The small number of parameters that do not meet both criteria are discussed below. The values of the parameters determined in the final fit are given with their standard deviations in Table 1. It is reassuring to note that the actual values obtained for the parameters were generally insensitive (within the experimental uncertainties) to the weighting scheme adopted in the fit, presumably because of the large size of the data set. The least-squares fit file, which contains the measured transition frequencies, their uncertainties, assignments and residuals between measured frequencies and those calculated from the final set of spectroscopic parameters, is provided as supplementary material.

4.3. Parameters determined in the fit

The millimetre-wave observations have allowed energy levels of NF_2 to be measured to significantly higher values of N and K_a. As a result, it has been possible to determine the sextic centrifugal parameters and also the centrifugal distortion corrections to the spin–rotation coupling for the first time. The rotational and centrifugal distortion Hamiltonians have been cast in the S-reduced form [22]. As in previous work, the scalar hyperfine parameters (a_F) and tensorial (dipolar; T_{ij}) electron spin–nuclear spin coupling terms for both ^{14}N and ^{19}F nuclei as well as the nuclear electric quadrupole coupling terms χ_{ii} for the ^{14}N nucleus have been determined in the fit. In particular, the parameter T_{ab}, which perturbs hyperfine levels with $\Delta K_a = 1$, $\Delta K_c = 0$, 2, and $\Delta N \leqslant 2$ that are accidentally degenerate and thus mixes *ortho* and *para* levels, has been determined for the first time. Centrifugal distortion corrections to the electron spin–nuclear spin coupling terms of ^{19}F were investigated in the present fit. Although such terms have been used rarely in the past, a complete set of quartic terms has been determined for the OBrO molecule [24]. These terms can be defined by analogy to the electron spin-rotation distortion terms [25]. Only one such term, $d_1^{SS}(F)$, the coefficient of $N^2(I_+S_+ + I_-S_-)$, was determined with significance in the present fit. Inclusion of further terms up to the complete set of six quartic terms yielded reasonable uncertainties for these parameters but they were not determined with significance and did not affect the rms error of the fit noticeably. The nuclear spin-rotation parameters C_{ii} for the ^{19}F nuclei were also tested in the fit. The inclusion of C_{bb} and C_{cc} had a very small effect on the rms error of the fit. However, since they were determined with significance and were of reasonable magnitude, they were retained in the final fit. The off-diagonal term $C_{ab} + C_{ba}$ had an insignificant effect. The corresponding diagonal terms for ^{14}N were also insignificant. The nuclear spin–nuclear spin coupling term S between the two ^{19}F nuclei was calculated from the structure and kept fixed in the fit. Its effect was minute; the largest effects

Table 1
Spectroscopic parameters[a] (MHz) of NF_2 in its ground $^2B_1$ state

Parameter	Value	Previous value [9]
A	70496.2977 (37)	70496.3339 (74)
B	11872.31537 (65)	11872.3162 (24)
C	10136.34816 (72)	10136.3594 (30)
D_K	1.898651 (92)	1.8953 (12)
$D_{NK} \times 10^3$	−52.7983 (145)	−51.61 (21)
$D_N \times 10^3$	14.07650 (106)	14.110 (15)
$d_1 \times 10^3$	−2.79359 (85)	−2.7360 (30)
$d_2 \times 10^6$	−243.535 (242)	−245.4 (27)
$H_K \times 10^6$	264.14 (222)	
$H_{KN} \times 10^6$	−33.022 (290)	
$H_{NK} \times 10^6$	0.915 (32)	
$h_1 \times 10^9$	43.40 (123)	
$h_2 \times 10^9$	−20.17 (41)	
$h_3 \times 10^9$	4.641 (81)	
ε_{aa}	−951.8864 (136)	−951.799 (22)
ε_{bb}	−92.9736 (52)	−92.9866 (94)
ε_{cc}	4.4503 (54)	4.4075 (87)
$D_K^S \times 10^3$	48.12 (49)	
$D_N^S \times 10^6$	135.2 (47)	
$d_1^S \times 10^6$	75.32 (168)	
$a_F(^{14}N)$	46.6082 (129)	46.609 (35)
$T_{aa}(^{14}N)$	−47.7068 (244)	−47.689 (39)
$T_{bb}(^{14}N)$	−50.4761 (162)	−50.472 (33)
$T_{cc}(^{14}N)$[b]	98.1829 (156)	98.161 (34)
$\chi_{aa}(^{14}N)$	5.556 (41)	5.495 (87)
$\chi_{bb}(^{14}N)$	−0.710 (27)	−0.667 (47)
$\chi_{cc}(^{14}N)$[b]	−4.846 (23)	−4.828 (40)
$a_F(^{19}F)$	164.5305 (151)	164.445 (42)
$T_{aa}(^{19}F)$	−241.9666 (301)	−241.724 (40)
$T_{bb}(^{19}F)$	−226.3361 (232)	−226.440 (41)
$T_{cc}(^{19}F)$[b]	468.3027 (241)	468.164 (48)
$\lvert T_{ab}(^{19}F)\rvert$	23.0 (33)	
$d_1^{SS}(^{19}F) \times 10^3$	0.220 (44)	
$C_{aa}(^{19}F) \times 10^3$	191.1 (111)	
$C_{bb}(^{19}F) \times 10^3$	26.3 (37)	
$C_{cc}(^{19}F) \times 10^3$	23.6 (38)	
$S(F–F) \times 10^3$	−11[c]	

[a] Watson's S-reduction was employed in the I^r representation. Numbers in parentheses are one standard deviation in units of the least significant figures.
[b] Derived value.
[c] Parameter constrained to this calculated value in the least-squares fit.

of 6 kHz on the transitions in the final fit occurred in some hyperfine components of the 2_{11}–2_{02} transition. It was retained in the fit to minimize effects on T_{ab}. The largest effect of the latter parameter occurred in the 3_{12}–3_{03} and 2_{11}–2_{02} transitions and amounted to at most 42 and 30 kHz, respectively. In this context it is worth mentioning that the largest effects of d_1^{SS}(F) were, at 32 kHz, almost as large. The ^{19}F nuclear spin-rotation terms had even larger effects of more than 100 kHz in several hyperfine components of 2_{11}–2_{02} and still more than 50 kHz for a few other transitions.

5. Discussion

5.1. Spectroscopic parameters

Additional measurements of the rotational spectrum of NF_2 in its ground vibrational level have been made in the millimetre-wave region between 95 and 179 GHz. The transitions are intrinsically weak because of the small electric dipole moment. Despite this, many higher-lying rotational levels have been accessed in these experiments. When the frequencies of these transitions are combined with the previous measurements of the rotational spectrum [8,9], it has proved possible to determine several of the higher order centrifugal distortion correction terms thereby making the determination of the main rotational, fine and hyperfine parameters more reliable. The best available previous set of parameters, those determined by Frank and Hüttner [9], are given in Table 1 for comparison; they have been converted to the values for the *S*-reduced form of the Hamiltonian [22]. It can be seen that the parameters in the present paper are significantly more precise.

5.2. Structural parameters

The rotational constants can be used to derive an experimental geometry of the molecule. The r_0 effective ground state structure, given in Table 2, is essentially unaltered from that determined earlier by Brown et al. [8]. However, the r_0 geometry is not the ultimate structure because vibrational contributions cause the rotational constants to differ from their equilibrium values. Subtleties in the fitting procedure or in the choice of isotopic species can cause considerable differences in the derived structure amounting to several times 0.1 pm or 0.1° even under favourable circumstances. A complete set of $3n-6$ vibrational corrections α_i^g, needed in first order for each rotational constant and each isotopic species of a non-linear *n*-atomic molecule, is rarely available from experiment even if, for a symmetric triatomic molecule such as NF_2, only three vibrations of one isotopic species have to be considered. Experimental information on the vibrational dependence of the rotational constants of NF_2 is available from the infrared studies of the ν_1 [4] and ν_3 bands [5]; there is as yet no information on the vibrational dependence of ν_2. *Ab initio* calculations provide a way to circumvent the lack of experimental data. The computation of the cubic force field, required to calculate the α_i^g parameters [26], is a major undertaking since small deficiencies in the *ab initio* method can produce sizeable errors in the cubic force field. Despite this, when the mixed experimental/*ab initio* equilibrium rotational constants are obtained from such a calculation, they are often a good enough approximation to the true values because the differences between ground and equilibrium rotational constants are generally small, of the order of one percent. The difference between ground state and equilibrium rotational constants can be expressed as [27]

$$B_e^g - B_0^g = -\frac{1}{2}\sum_i d_i \alpha_i^g \tag{9}$$

if one neglects the higher order corrections which are much smaller. Here *g* stands for the three rotational constants *A*, *B*, and *C*, d_i is the degeneracy of the vibration ν_i and *i* runs over the normal coordinates. In the present case each of the three vibrational modes is non-degenerate.

Table 2 gives the ground state rotational constants as well as the equilibrium values. The latter are calculated from the experimental zero-point rotational constants in two ways: (i) using the experimental values for α_i^g with $i = 1$ and 3 and the *ab initio* value estimated for α_2^g and (ii) using the *ab initio* values for all the required α_i^g values. The *ab initio* calculations were done at the MP2 and B3LPY levels, employing the moderately large basis set aug-cc-pwCVTZ. The inertial defects, the calculated bond lengths and bond angles are also given in the table. As can be seen, the vibrational corrections to *B* and *C* are about 1% while those for *A* are even smaller. The small inertial defect $\Delta = I_c - I_b - I_a$ for the zero-point level is consistent with these small corrections. The calculated equilibrium values for Δ are very small and negative, as expected. The electronic contribution to the inertial defect is generally small and positive [27]; a calculation of this contribution from the rotational *g*-factors [9] puts it at 0.00227 (11) amu Å^2. This suggests that the equilibrium inertial defects in Table 2 calculated with purely *ab initio* corrections are fortuitously close to zero. In contrast, the equilibrium inertial defect derived from the available experimental data is slightly too negative.

The quality of the mixed experimental/*ab initio* structural parameters is limited by the accuracy with which the $B_e^g - B_0^g$ values are calculated because the experimental B_0^g values have been

Table 2
Rotational parameters[a] B^g (MHz), inertial defect Δ (amu Å^2), and structural parameters *r*, ∠(pm, deg) of NF_2 in the ground vibrational state and mixed experimental/*ab initio* equilibrium values

	Ground state	Equilibrium state[b]		
		α(MP2)[c]	α(B3LYP)[d]	α(exptl)[e]
A	70496.298	70413.473	70446.018	70519.43
B	11872.3323	11943.9851	11948.7187	11953.07
C	10136.3298	10211.8381	10216.0822	10221.83
Δ	0.121516	−0.000209	−0.000999	−0.005642
r	134.9	134.723	134.695	134.655
∠	103.35	103.1245	103.1262	103.144

[a] Reduction-free values [22].
[b] Preferred structure: $r = 134.691$ (68) pm, $\angle = 103.132$ (20)°, the average of all three determinations, see Section 5.2.
[c] $B_e^g - B_0^g$ from MP2/aug-cc-pwCVTZ *ab initio* calculation.
[d] $B_e^g - B_0^g$ from B3LYP/aug-cc-pwCVTZ *ab initio* calculation.
[e] Experimental values obtained using the experimental values for α_i^g with $i = 1$ and 3 (see Table 3) together with the *ab initio* values for α_2^g; *g* stands for the rotational constants, *A*, *B*, and *C*.

Table 3
Comparison between experimental values for the vibration–rotation interaction terms α_i^B (MHz) with those calculated *ab initio*

Parameter	Experimental[a]	MP2[b]	B3LYP[b]	
		aCTZ	aCTZ	aCQZ
α_1^A	83.60 (15)	194.90	167.87	166.43
α_1^B	−64.490 (59)	−56.81	−58.97	−59.65
α_1^C	−6.077 (71)	−2.23	−7.80	−8.10
α_2^A	—	643.38	637.60	640.90
α_2^B	—	−37.48	−39.60	−39.92
α_2^C	—	−52.42	−54.29	−54.51
α_3^A	−770.35 (13)	−672.63	−704.92	−718.40
α_3^B	−58.449 (41)	−49.02	−54.20	−54.96
α_3^C	−111.570 (49)	−96.34	−97.41	−98.56

[a] Effective experimental values for α_i^g parameters have been obtained by re-fitting the infrared data from Refs. [4,5] with the ground state parameters constrained to the values determined in the present work. The numbers in parentheses are one standard deviation in units of the least significant figures.
[b] Determined from $B_e^g - B_0^g$; see also Section 5.2. The basis set descriptions aCXZ stand for aug-cc-pwCVXZ with X = T, Q; see Section 3.

determined much more accurately (to one part in 10^8). Table 3 gives experimental values for the parameters α_i^g together with the theoretical values. The former have been obtained from a least-squares re-fit of the infrared data from Refs. [4,5], constraining the ground state parameters to the values determined in the present work (given in Table 1). The agreement between theory and experiment is only fairly good. At least some of the differences are caused by the fact that the experimental values are derived simply from the differences $B_1^g - B_0^g$; they thus neglect contributions from the higher order parameters $\gamma_{i,j}^g$ that are currently unavailable. These corrections may well amount to some tens of megahertz for *A* and to a few megahertz for *B* and *C*. In contrast, the theoretical calculations provide true α_i^g values but their quality is usually limited by the method of the calculation and, to a lesser amount, by the finite size of the basis set. The comparison between the B3LYP and MP2 values shows that limitations of the methods account for similar or maybe even larger deviations. In this context it is interesting to note that the B3LYP values are generally better than the MP2 values. In contrast, the finite basis set size produces much smaller deviations as demonstrated by the two B3LYP calculations.

Even though the various sets of α_i^g parameters differ somewhat, the resulting equilibrium rotational constants are closely similar as are the derived equilibrium structural parameters given in Table 2. The use of larger basis sets for the calculation of $B_e^g - B_0^g$ results in changes of the derived structural parameters that are much smaller than the differences between the two methods. Since each set of equilibrium structural parameters has some limitations, we use the average of the three sets of parameters as the preferred structure and the range of values as a conservative estimate of the uncertainty.

Structural parameters as well as the dipole moment have been calculated *ab initio* using the B3LYP, MP2, and CCSD(T) methods; the results are summarised in Table 4 where the experimental values are also given for comparison. The bond lengths are already fairly close to the basis set limit at basis sets of triple zeta quality as expected for molecules consisting of fairly light elements. Use of a quadruple zeta basis set produces a slightly shorter bond length; further extension of the basis set has only marginal effects as evaluated at the B3LYP level. All bond lengths are rather close to the experimental values; the B3LYP values are slightly longer, the MP2 values slightly shorter, while the CCSD(T) values are very close. There seem to be no clear general trends for B3LYP structure calculations. However, the performances of MP2 and CCSD(T) are in line with general trends if the basis sets are sufficiently large, namely MP2 bond lengths tend to be shorter than experiment for sufficiently large basis sets while CCSD(T) bond lengths are very close, sometimes just barely shorter than experiment. One set of diffuse basis functions lengthens the NF bond distance as one would expect for a molecule consisting only of electronegative elements. A second set of diffuse basis functions or core-correlating basis functions have small to negligible effects. However, correlation of all electrons at the MP2 or CCSD(T) level causes a shortening of the bond length as is commonly observed. The calculated bond angles are slightly larger than the experimental value throughout all basis sets for the B3LYP and MP2 calculations, but the CCSD(T) values approach the experimental one. The bond angle shows only minute basis set dependence for B3LYP calculations; increased electron correlation causes somewhat larger effects. The largest effect occurs for the addition of a first set of diffuse basis functions. The same holds for the calculated dipole moments. It should be pointed out all MP2 dipole moment values have been obtained at the MP2 density although the values are calculated at the SCF density by default. In the case of NF_2, these values are around 0.4 D, much larger than the experimental values. Dipole moments calculated at the SCF density are also available for CCSD(T) calculation.

Table 4
Equilibrium structural parameters *r*, ∠(pm, deg) and dipole moment μ (D) of NF_2 calculated *ab initio* in comparison with experimental values

Method[a]	*r*	∠	μ
B3LYP			
cc-pVTZ	135.46	103.48	0.084
aug-cc-pVTZ	135.52	103.45	0.124
daug-cc-pVTZ	135.52	103.45	0.120
aug-cc-pwCVTZ	135.52	103.45	0.124
cc-pVQZ	135.38	103.48	0.095
aug-cc-pwCVQZ	135.31	103.52	0.110
aug-cc-pwCV5Z	135.27	103.47	0.109
MP2			
cc-pVTZ	134.19	103.56	0.084
aug-cc-pVTZ	134.52	103.34	0.134
aug-cc-pwCVTZ	134.50	103.40	0.134
aug-cc-pwCVTZ(ae)	134.26	103.40	0.123
cc-pVQZ	133.95	103.48	0.089
aug-cc-pwCVQZ	134.01	103.38	0.110
aug-cc-pwCVQZ(ae)	133.80	103.45	0.100
CCSD(T)			
cc-pVTZ	134.97	103.30	–
aug-cc-pVTZ	135.34	103.07	–
aug-cc-pCVTZ	135.29	103.09	–
aug-cc-pwCVTZ(ae)	135.08	103.08	–
cc-pVQZ	134.71	103.24	–
aug-cc-pwCVQZ	134.77	103.21	–
aug-cc-pwCVQZ(ae)[b]	134.64	103.22	–
Experimental[c]	134.69	103.13	0.136

[a] The method used is given first in a row by itself; the basis sets used with that method then follow below. The abbreviation ae in parentheses indicates correlation of all electrons; the electrons of the core are generally not correlated in MP2 or CCSD(T) calculations.
[b] Estimate based on trends in CCSD(T) and MP2 calculations.
[c] Structural parameters from this work, see also Table 2 and Section 5.2. Dipole moment from Ref. [8].

However, these values are still slightly larger than the MP2 values. For that matter, no dipole moments are given for the CCSD(T) calculations and only values calculated at the MP2 density for calculations with this method. The dipole moment values given in Table 4 are close to the experimental value, especially when diffuse basis functions were used in the calculations. Overall, the available CCSD(T) values are very close to the experimental ones, thereby justifying the use of average values of the two theoretical methods presented in Table 2 as preferred values. The very good agreement between the experimental and CCSD(T) values suggests that the estimated errors reported for the preferred structural parameters may be quite conservative.

As one can also see in Table 2, the computed ground-state bond length and the bond angle are about 0.2 pm and 0.2° larger than the experimental values. Table 5 summarises NF bond lengths for several molecular species and obtained by various means. The NF_2 value of 134.7 pm is between that of NF, 131.7 pm in the electronic ground state and the NF_3 value of 136.5 pm, closer to the latter. Cationic species such as NF_4^+, N_2F^+ and NF^+ show much shorter NF bond lengths because there are fewer electrons in anti-bonding orbitals. This shortening seems to be more pronounced for smaller species. It should be pointed out that rotational spectroscopy in combination with *ab initio* calculations [29] seems to indicate that interactions with the anion in the solid state shortens the NF bond length in N_2FAsF_6 compared with the free N_2F^+ cation. As with cationic species, electropositive substituents on the nitrogen atom cause a pronounced lengthening of the NF bond as can be seen in the trend from NF_3 over NHF_2 to NH_2F, where the NF bond lengths are 136.5, 140.0, and 143.2 pm, respectively. Similar effects occur for substituents capable of π-bonding; a larger amount of π-bonding and a smaller system seems to weaken the NF bond most so

Table 5
NF bond lengths (pm) of NF_2 in comparison with other, selected molecular species determined by microwave spectroscopy (MW)[a], electron diffraction (ED)[b], or single crystal X-ray diffraction (X!)

Species	MW (r_e)	MW (r_0)	ED	X!	Ref.
NF^+	118.0 (6)				[28][c]
N_2F^+	124.61 (10)			121.7	[29][d],[30][e]
NF, $b\ ^1\Sigma^+$	129.98374 (17)				[31][f]
NF, $a\ ^1\Delta$	130.39563 (17)				[31][f]
NF_4^+				130.76 (16)	[32][g]
NF, $X\ ^3\Sigma^-$	131.698 (9)				[31][h]
NF_2	134.691 (68)	134.94	136.3 (8)		TW[i],[8][j],[33]
NF_3	136.48 (20)	137.1			[34,35][j]
N_2F_4			139.3 (8)		[33]
trans-N_2F_2			139.6 (8)		[3]
cis-N_2F_2		138.4 (10)	141.0 (9)		[37,36]
NHF_2		140.0 (2)		139.4 (4)	[38,39][k]
ONF_3			143.2 (2)		[40]
NH_2F		143.29 (3)			[41]
N_3F		144.4 (10)			[42][l]
FNO_2	145.60 (28)	146.7 (15)			[43,44]
FNO	151.658 (25)				[45]

[a] r_e and r_0 refer to equilibrium and ground state values, respectively.
[b] Vibrationally averaged bond length, r_a.
[c] From photoelectron spectroscopy of NF.
[d] Mixed experimental/*ab initio* value assuming r_e(NN) = 110.34 (5) pm; the uncertainty for the NF bond length is assumed.
[e] N_2FAsF_6; r(NF) and r(NN) could not be separated experimentally; 231.6 (12) pm was determined for the sum; *ab initio* ratios were used to derive individual bond lengths.
[f] Second (b) and first (a) excited electronic state, respectively.
[g] NF_4BF_4; average of two close values, 130.79 (13) and 130.73 (13) pm.
[h] Ground electronic state.
[i] This work.
[j] No uncertainties have been given.
[k] Determined at −150 °C; average of two close values, 139.6 (2) and 139.2 (2) pm.
[l] Substitution structure (r_s).

Table 6
Nuclear hyperfine parameters (MHz) and the angle between the a-axis and the z'-axis of the spin–spin coupling tensor (deg) for NF_2 and NH_2 in their $^2B_1$ ground states

Parameter	NF_2[a]	NH_2[b]
$a_F(^{14}N)$	46.608 (13)	28.050 (11)
$T_{aa}(^{14}N)$	−47.707 (24)	−43.188 (17)
$T_{bb}(^{14}N)$	−50.476 (16)	−44.464 (19)
$T_{cc}(^{14}N)$[c]	98.183 (16)	87.652 (16)
$\chi_{aa}(^{14}N)$	5.556 (41)	0.366 (31)
$\chi_{bb}(^{14}N)$	−0.710 (27)	−3.833 (37)
$\chi_{cc}(^{14}N)$[c]	−4.846 (23)	3.466 (24)
$a_F(^{19}F/H)$	164.531 (15)	−67.170 (12)
$T_{aa}(^{19}F/H)$	−241.967 (30)	18.359 (22)
$T_{bb}(^{19}F/H)$	−226.336 (23)	−13.211 (25)
$T_{cc}(^{19}F/H)$[b] = T_y	468.303 (24)	−5.148 (19)
$\lvert T_{ab}(^{19}F/H)\rvert$	23.0 (33)	58.5 (25)[c]
$T_{z'}(^{19}F/H)$	−258.4 (31)	63.2 (24)
$T_{x'}(^{19}F/H)$	−209.9 (31)	−58.0 (24)
$\Theta_{az'}(^{19}F/H)$[d]	35.62 (144)	37.45 (32)

[a] Values from present work.
[b] Values determined by Müller et al. [46], Gendriesch et al. [47].
[c] Value determined indirectly from a study of NHD by Steimle et al. [48] from the isotopic shifts of the T_{ii} tensor.
[d] $\Theta_{az'}$ is the angle between the principal axis z' of the ^{19}F dipolar tensor and the a inertial axis. For comparison, the N–F bond makes an angle Θ_{az} of 38.4° with the a-axis.

that it is very long in FNO_2 for example and even longer still in FNO at 151.7 pm.

5.3. Hyperfine parameters

A complete set of hyperfine parameters for both the ^{14}N and ^{19}F nuclei has been determined; this includes the first determination of the off-diagonal dipole–dipole term T_{ab} for ^{19}F. The molecule that is most closely related to NF_2 is NH_2. The primary hyperfine parameters for these two molecules in the zero-point level of their $^2B_1$ ground states are given in Table 6. It can be seen that, while the magnetic hyperfine parameters for the ^{14}N nucleus are fairly similar, the electric quadrupole parameters are not. The magnetic hyperfine parameters depend on the spatial distribution of the unpaired electron which, to a first approximation, occupies the $2p_y$ orbital on the N atom in both molecules (y is the out-of-plane axis). The dipolar interaction broadly reflects the cylindrical symmetry of this 2p orbital; the small, non-zero magnitude of the Fermi contact parameter arises from configuration interaction. The ^{14}N electric quadrupole interaction on the other hand depends on the electric field gradient produced by nearby charges; the electron charge distribution is significantly different for NF_2 as becomes obvious when we turn attention to the hyperfine parameters associated with the H or F nuclei. Given that both of these nuclei have $I = 1/2$ and very similar g-factors (5.5857 and 5.2578, respectively), one might naively expect the magnetic hyperfine parameters also to be similar. In reality, they are very different as can be seen in Table 6; there is no correspondence between the magnitudes or even the signs of the various parameters. The explanation for this difference lies in the composition of the b_1 molecular orbital that contains the unpaired electron. For NH_2, it is essentially a pure $2p_y$ orbital on the N atom. The dipole–dipole interaction therefore acts over the distance of the N–H bond length and is correspondingly weak; the negative Fermi contact interaction is a textbook example of spin polarisation as shown, for example, in CH [49] or NH [50]. For NF_2, on the other hand, the b_1 molecular orbital is a linear combination of $2p_y$ orbitals on each of the N and F atoms. Each ^{19}F nucleus therefore shows a larger dipole–dipole interaction that reflects the cylindrical symmetry of the $2p_y$ orbital. The Fermi contact interaction on the ^{19}F nucleus is again a manifestation of configuration interaction but with different character in this case.

Previous attempts to determine the off-diagonal dipole–dipole term T_{ab} in the spectra of NH_2 [46,47], PH_2 [51], and AsH_2 [52,53] did not succeed, despite accessing the nearly degenerate *ortho*/*para* pair of levels N_{0N} and N_{1N}. NF_2 was considered a better candidate molecule for such a determination because of the large magnetic moment of the ^{19}F nucleus and the fact that the rotational levels are closer together than in a dihydride. The objective has been achieved but only just because it turns out that the parameter is small in magnitude (23.0 ± 3.3 MHz). The reason for this is that the b_1 molecular orbital shows predominantly $2p_y$ character in the region of the ^{19}F nucleus. With this simplistic picture of the unpaired electron, the components of the dipolar tensor in the local coordinate system (with the z axis lying along the N–F bond) are $T_{xx} = T_{zz} = -1/2T_{yy}$, $T_{xz} = 0$. This cylindrical symmetry is unaffected by any rotation in the molecular plane and consequently T_{ab} is also zero. The magnitude of the value determined for T_{ab} therefore gives information about the deviation of the electron wavefunction from cylindrical symmetry at the F nucleus. We can use the values determined for the parameters T_{ij} ($i, j = a, b, c$) in the present work to establish the principal components of the dipolar tensor and the alignment of its axes relative to the (x, y, z) axis system; the latter is parallel and perpendicular to the N–F bond. The results are also given in Table 6. It can be seen that there is a small but significant difference (2.8°) between the orientations of the principal and (x, y, z) coordinate systems.

Table 7 summarises electron spin–nuclear spin coupling parameters calculated for the ^{19}F nuclei with the B3LYP and MP2 methods employing a number of moderately large to large basis sets.

Table 7
^{19}F spin–spin coupling constants of NF_2 calculated *ab initio* in comparison with experimental values

Method[a]	a_F	T_{aa}	T_{bb}	T_{cc}	$\lvert T_{ab}\rvert$
B3LYP					
cc-pVTZ	120.4	−258.7	−242.3	501.0	9.8
aug-cc-pVTZ	98.6	−253.0	−235.7	488.7	9.6
daug-cc-pVTZ	97.0	−253.1	−235.7	488.8	9.7
aug-cc-pwCVTZ	131.7	−258.1	−240.2	498.3	10.1
cc-pVQZ	99.2	−261.1	−243.6	504.6	9.8
aug-cc-pVQZ	98.1	−259.1	−241.1	500.3	9.5
aug-cc-pwCVQZ	140.4	−264.0	−245.4	509.4	10.0
aug-cc-pV5Z	121.9	−263.2	−244.7	508.0	10.0
aug-cc-pwCV5Z	141.8	−266.2	−247.5	513.6	10.4
MP2					
cc-pVTZ	143.1	−223.9	−222.7	446.7	20.4
aug-cc-pVTZ	119.9	−217.3	−216.6	443.8	23.7
aug-cc-pwCVTZ	165.1	−219.6	−219.0	438.8	23.7
aug-cc-pwCVTZ(ae)	169.0	−221.5	−220.3	441.8	20.8
cc-pVQZ	136.2	−224.0	−223.8	447.9	23.2
aug-cc-pwCVQZ	175.1	−224.9	−224.7	449.6	24.7
aug-cc-pwCVQZ(ae)	179.9	−226.8	−226.0	452.7	22.0
Experimental	164.5	−242.0	−226.3	468.3	23.

[a] The method used is given first in a row by itself; the basis sets used with that method then follow below. The abbreviation ae in parenthesis indicates correlation of all electrons; the electrons of the core are generally not correlated.

Table 8
^{14}N spin–electron spin coupling constants of NF_2 calculated *ab initio* in comparison with experimental values

Method[a]	a_F	T_{aa}	T_{bb}	T_{cc}
B3LYP				
cc-pVTZ	29.8	−46.3	−49.4	95.6
aug-cc-pVTZ	25.8	−46.7	−49.6	96.3
daug-cc-pVTZ	24.9	−46.7	−49.6	96.3
aug-cc-pwCVTZ	39.6	−48.1	−51.2	99.3
cc-pVQZ	30.0	−47.9	−51.0	98.9
aug-cc-pVQZ	31.1	−47.9	−51.1	99.0
aug-cc-pwCVQZ	44.0	−49.0	−52.3	101.3
aug-cc-pV5Z	39.7	−48.8	−52.0	100.8
aug-cc-pwCV5Z	44.0	−49.4	−52.6	101.9
MP2				
cc-pVTZ	22.5	−46.8	−50.3	97.1
aug-cc-pVTZ	22.0	−47.2	−50.4	97.6
aug-cc-pwCVTZ	38.5	−48.1	−51.4	99.5
aug-cc-pwCVTZ(ae)	41.5	−48.3	−51.6	99.9
cc-pVQZ	28.2	−48.1	−51.4	99.5
aug-cc-pwCVQZ	40.7	−49.0	−52.4	101.4
aug-cc-pwCVQZ(ae)	44.5	−49.3	−52.6	101.9
Experimental	46.6	−47.7	−50.5	98.2

[a] The method used is given first in a row by itself; the basis sets used with that method then follow below. The abbreviation ae in parenthesis indicates correlation of all electrons; the electrons of the core are generally not correlated.

The scalar values a_F display the usual pronounced basis set dependence which decreases considerably once the basis sets contain core-correlating basis functions. The change from quadruple to quintuple basis set produces almost negligible effects with both methods, indicating that convergence has essentially been achieved whereas a marked change is calculated without these basis functions. The B3LYP value calculated with the largest basis set is still smaller than the experimental one by about 15% while the corresponding MP2 value is about 10% larger.

In contrast to the scalar values, the dipolar values T_{ij} show only small variations with basis sets. The diagonal values calculated with both methods are quite similar to the experimental ones; the B3LYP values are slightly larger in magnitude while the MP2 values are slightly smaller, except for T_{bb}, which is very close. It is interesting to note that the difference between T_{aa} and T_{bb} is very similar to the experimental values for the B3LYP calculations whereas for the MP2 calculations, it is much smaller. In contrast, the MP2 values for the off-diagonal T_{ab} term are in very good agreement with the experimental one whereas the B3LYP values are only about half as large. These deviations result in very different angles between the z-axis of the spin–spin coupling tensor and the a-axis of the inertial tensor: The B3LYP and MP2 calculations yield values near 24° and 45°, respectively, with the experimental value of 35.6 (14)° being almost halfway between. This value is also very close to the angle between the NF bonds and the a-axis which amounts to 38.4°.

Table 8 provides the corresponding spin–spin coupling parameters for the ^{14}N nucleus for reasons of completeness. As can be seen, the scalar values again show large variations with basis sets whereas the dipolar values are fairly basis-set independent. Both methods yield similar values that are close to experiment, especially for the largest basis sets.

6. Conclusions

Many new measurements of lines in the millimetre-wave spectrum of the NF_2 radical in the zero-point level of its ground $^2B_1$ state have been made and assigned. The measurements, together with those made previously [8,9], have been subjected to a least-squares fit to determine several higher order centrifugal distortion parameters, thereby determining the rotational and spin-rotational parameters more securely. It has also been possible to determine the parameter T_{ab} in the electron spin ^{19}F spin dipolar interaction for the first time. This term causes a mixing of *ortho* and *para* levels. The analysis has been accompanied by high level *ab initio* calculations which produce results close to those obtained from experiment and also allow the accurate determination of the equilibrium geometry. The line, parameter and fit files generated in the course of the present investigation are available in the Fitting Spectra section of the Cologne Database for Molecular Spectroscopy (CDMS) [54,55] at http://www.astro.uni-koeln.de/vorhersagen/pickett/beispiele/NF2/.

Acknowledgments

We much appreciate the computer programming of W. Deckenbach, which was used to analyse the millimetre-wave spectra in the early stages. H.S.P.M. is grateful for support by the Bundesministerium für Bildung und Forschung (BMBF), administered through Deutsches Zentrum für Luft- und Raumfahrt (DLR; the German space agency). The same agency also provides support for the CDMS.

Appendix A. Supplementary data

Supplementary data for this article are available on ScienceDirect (www.sciencedirect.com) and as part of the Ohio State University Molecular Spectroscopy Archives (http://library.osu.edu/sites/msa/jmsa_hp.htm). Supplementary data associated with this article can also be found, in the online version, at doi:10.1016/j.jms.2008.02.014.

References

[1] F.A. Johnson, C.B. Colbourn, J. Am. Chem. Soc. 83 (1961) 3043–3047.
[2] M.D. Harmony, R.J. Myers, L.J. Schoen, D.R. Lide, D.E. Mann, J. Chem. Phys. 35 (1961) 1129–1130.
[3] M.D. Harmony, R.J. Myers, J. Chem. Phys. 37 (1962) 636–641.
[4] P.B. Davies, P.A. Hamilton, W. Lewis-Bevan, D.K. Russell, Proc. R. Soc. A392 (1984) 445–455.
[5] P.B. Davies, P.A. Hamilton, Proc. R. Soc. A393 (1984) 397–408.
[6] K. Hakuta, H. Uehara, J. Chem. Phys. 374 (1981) 5995–5999.

[7] L.W. Hrubesh, E.A. Rinehart, R.E. Anderson, J. Mol. Spectrosc. 36 (1970) 354–356.
[8] R.D. Brown, F.R. Burden, P.D. Godfrey, I.R. Gillard, J. Mol. Spectrosc. 25 (1974) 301–321.
[9] U.E. Frank, W. Hüttner, Chem. Phys. 152 (1991) 261–279.
[10] W. Hüttner, Chem. Phys. Lett. 53 (1978) 369–373.
[11] H. Uehara, K. Horiai, J. Chem. Phys. 84 (1986) 5568–5574.
[12] R.F. Curl, J.V.V. Kasper, K.S. Pitzer, J. Chem. Phys. 46 (1967) 3220–3228.
[13] D. Chadwick, D.J. Millen, Trans. Faraday Soc. 67 (1971) 1551–1568.
[14] H.S.P. Müller, C.E. Miller, E.A. Cohen, Angew. Chem. 108 (1996) 2285–2288;
H.S.P. Müller, C.E. Miller, E.A. Cohen, Angew. Chem. Int. Ed. Engl. 35 (1996) 2129–2131.
[15] H.S.P. Müller, E.A. Cohen, J. Chem. Phys. 106 (1997) 8344–8354.
[16] U.E. Frank, Doctoral Thesis, University of Ulm, 1991.
[17] T.H. Dunning Jr., J. Chem. Phys. 90 (1989) 1007–1023.
[18] R.A. Kendall, T.H. Dunning Jr., R.J. Harrison, J. Chem. Phys. 96 (1992) 6796–6806.
[19] D.E. Woon, T.H. Dunning Jr., J. Chem. Phys. 100 (1994) 2975–2988.
[20] K.A. Peterson, T.H. Dunning Jr., J. Chem. Phys. 117 (2002) 10548–10560.
[21] M.J. Frisch, G.W. Trucks, H.B. Schlegel, G.E. Scuseria, M.A. Robb, J.R. Cheeseman, J.A. Montgomery Jr., T. Vreven, K.N. Kudin, J.C. Burant, J.M. Millam, S.S. Iyengar, J. Tomasi, V. Barone, B. Mennucci, M. Cossi, G. Scalmani, N. Rega, G.A. Petersson, H. Nakatsuji, M. Hada, M. Ehara, K. Toyota, R. Fukuda, J. Hasegawa, M. Ishida, T. Nakajima, Y. Honda, O. Kitao, H. Nakai, M. Klene, X. Li, J.E. Knox, H.P. Hratchian, J.B. Cross, C. Adamo, J. Jaramillo, R. Gomperts, R.E. Stratmann, O. Yazyev, A.J. Austin, R. Cammi, C. Pomelli, J.W. Ochterski, P.Y. Ayala, K. Morokuma, G.A. Voth, P. Salvador, J.J. Dannenberg, V.G. Zakrzewski, S. Dapprich, A.D. Daniels, M.C. Strain, O. Farkas, D.K. Malick, A.D. Rabuck, K. Raghavachari, J.B. Foresman, J.V. Ortiz, Q. Cui, A.G. Baboul, S. Clifford, J. Cioslowski, B.B. Stefanov, G. Liu, A. Liashenko, P. Piskorz, I. Komaromi, R.L. Martin, D.J. Fox, T. Keith, M.A. Al-Laham, C.Y. Peng, A. Nanayakkara, M. Challacombe, P.M.W. Gill, B. Johnson, W. Chen, M.W. Wong, C. Gonzalez, J.A. Pople, Gaussian 03, Revision B.04, Gaussian, Inc., Pittsburgh, PA, 2003.
[22] J.K.G. Watson, in: J.R. Durig (Ed.), Vibrational Spectra and Structure, vol. 6, Elsevier, 1977, pp. 1–89.
[23] H.M. Pickett, J. Mol. Spectrosc. 148 (1991) 371–377.
[24] H.S.P. Müller, C.E. Miller, E.A. Cohen, J. Chem. Phys. 107 (1997) 8292–8302.
[25] J.M. Brown, T.J. Sears, J. Mol. Spectrosc. 75 (1979) 111–133.
[26] I.M. Mills, in: K.N. Rao, C.W. Mathews (Eds.), Molecular Spectroscopy: Modern Research, Academic Press, New York, 1972, pp. 115–140.
[27] For example, W. Gordy, R.L. Cook, Microwave Molecular Spectra, third ed., Wiley, New York, 1984.
[28] J.M. Dyke, N. Jonathan, A.E. Lewis, A. Morris, J. Chem. Soc. Faraday Trans. 2 78 (1982) 1445–1450.
[29] P. Botschwina, P. Sebald, M. Bogey, C. Demuynck, J.-L. Destombes, J. Mol. Spectrosc. 153 (1992) 255–275.
[30] K.O. Christe, R.D. Wilson, W.W. Wilson, R. Bau, S. Sukumar, D.A. Dixon, J. Am. Chem. Soc. 113 (1991) 3795–3800.
[31] K. Kobayashi, S. Saito, J. Chem. Phys. 108 (1998) 6606–6610.
[32] R. Haiges, M. Gerken, A. Iuga, R. Bau, K.O. Christe, Inorg. Chem. 45 (2006) 7981–7984.
[33] R.K. Bohn, S.H. Bauer, Inorg. Chem. 6 (1967) 304–309.
[34] M. Otake, C. Matsumura, Y. Morino, J. Mol. Spectrosc. 28 (1968) 316–324.
[35] J. Sheridan, W. Gordy, Phys. Rev. 79 (1950) 513–515.
[36] R.K. Bohn, S.H. Bauer, Inorg. Chem. 6 (1967) 309–312.
[37] R.L. Kuczkowski, E.B. Wilson, J. Chem. Phys. 39 (1963) 1030–1034.
[38] D.R. Lide, J. Chem. Phys. 38 (1963) 456–460.
[39] M.F. Klapdor, H. Willner, W. Poll, D. Mootz, Angew. Chem. 108 (1996) 336; M.F. Klapdor, H. Willner, W. Poll, D. Mootz, Angew. Chem. Int. Ed. Engl. 35 (1996) 320.
[40] V. Plato, W.D. Hartford, K. Hedberg, J. Chem. Phys. 53 (1970) 3488–3494.
[41] D. Christen, R. Minkwitz, R. Nass, J. Am. Chem. Soc. 109 (1987) 7020–7024.
[42] D. Christen, H.-G. Mack, G. Schatte, H. Willner, J. Am. Chem. Soc. 110 (1988) 707–712.
[43] J. Demaison, A.G. Császár, A. Dehayem-Kamadjeu, J. Phys. Chem. A 110 (2006) 13609–13617.
[44] A.C. Legon, D.J. Millen, J. Chem. Soc. (A) (1968) 1736–1740.
[45] C. Degli Esposti, G. Cazzoli, P.G. Favero, J. Mol. Spectrosc. 109 (1985) 229–238.
[46] H.S.P. Müller, H. Klein, S.P. Belov, G. Winnewisser, I. Morino, K.M.T. Yamada, S. Saito, J. Mol. Spectrosc. 195 (1999) 177–184.
[47] R. Gendriesch, F. Lewen, G. Winnewisser, H.S.P. Müller, J. Mol. Struct. 599 (2001) 293–304.
[48] T.C. Steimle, J.M. Brown, R.F. Curl, J. Chem. Phys. 73 (1980) 2552–2558.
[49] M.C. McCarthy, S. Mohamed, J.M. Brown, P. Thaddeus, Proc. Natl. Acad. Sci. USA 103 (2006) 12263–12268.
[50] J. Flores-Mijangos, J.M. Brown, F. Matsushima, H. Odashima, K. Takagi, L.R. Zink, K.M. Evenson, J. Mol. Spectrosc. 225 (2004) 189–195.
[51] L. Margulès, E. Herbst, V. Ahrens, F. Lewen, G. Winnewisser, H.S.P. Müller, J. Mol. Spectrosc. 211 (2002) 211–220.
[52] H. Fujiwara, K. Kaori, O. Hiroyuki, S. Saito, J. Chem. Phys. 109 (1998) 5351–5355.
[53] R.A. Hughes, J.M. Brown, K.M. Evenson, J. Mol. Spectrosc. 200 (2000) 210–228.
[54] H.S.P. Müller, S. Thorwirth, D.A. Roth, G. Winnewisser, Astron. Astrophys. 370 (2001) L49–L52.
[55] H.S.P. Müller, F. Schlöder, J. Stutzki, G. Winnewisser, J. Mol. Struct. 742 (2005) 215–227.